BLAST PERFORMANCE OF LOAD-BEARING AND NON-LOAD-BEARING PRESTRESSED CONCRETE PANELS

Thomas J. Mander, P.E., Baker Engineering and Risk Consultants, Inc., San Antonio, TX
Michael J. Lowak, Baker Engineering and Risk Consultants, Inc., San Antonio, TX
Michael A. Polcyn, Baker Engineering and Risk Consultants, Inc., San Antonio, TX

ABSTRACT

This paper presents the experimental and analytical results for blast loaded prestressed concrete wall panels. Full scale, 16-ft simple-span, prestressed concrete wall panels were tested with blast loads generated from a shock tube. The panels tested included 6-inch thick solid prestressed concrete panels, and prestressed concrete sandwich panels with 3-inch thick wythes separated with 2 inches of rigid insulation. Panels were tested in both a non-load-bearing and load-bearing configuration. Load-bearing panels had a static concentric axial load applied throughout the dynamic shock tube tests. The axial load magnitude was 10 percent of the gross static axial capacity of each wall member using the nominal concrete compression strength. All panels had simple bearing connections without in-plane restraint. Panels were tested multiple times to define support rotations at which different levels of damage occurred.

Non-linear single-degree-of-freedom analyses of the experiments are presented in this paper. Comparisons are made using customary elastic-plastic resistance functions, as well as multi-linear resistance functions, accounting for the constitutive properties of plain concrete, prestressing steel, and axial load effects.

Keywords: Blast, Shock Tube, Prestressed Concrete Panels, Load-bearing, Response Criteria, Dynamic Analysis

INTRODUCTION

The blast analysis and design of buildings is most commonly performed at a component level, using single-degree-of-freedom (SDOF) methods. Individual components, such as wall panels, are analyzed for transient blast loads, and the peak deflection is calculated. The peak deflection is converted into an equivalent support rotation using the idealization shown in Fig. 1, which assumes plastic response of a simply-supported beam or panel. The support rotation is compared to prescriptive limits to determine the anticipated level of component damage.

Response limits currently exist for non-load-bearing prestressed concrete components. These values are conservative and have limited blast data to justify their values. While load-bearing prestressed concrete panels are widely used in conventional construction, their use in blast-resistant construction, particularly for government agencies, has been limited by the absence of response criteria. The use of sandwich panels has also been limited in blast-resistant construction by the lack of available blast performance criteria.

This paper provides an overview of research performed by BakerRisk under contract with PCI to develop SDOF models with supporting rational performance criteria that will allow the expanded use of load-bearing prestressed panels in blast-resistant construction. The analytical models and response limits are intended for far-range blast effects for panels behaving in flexure with static axial loads. The analytical models are validated with a series of shock tube tests, performed on full scale non-load-bearing and load-bearing panels. Panel construction included solid prestressed panels and prestressed sandwich panels. Load-bearing panels in this study support concentric axial loads with a magnitude of 10 percent of their gross static axial capacity ($0.1f'_cA_g$).

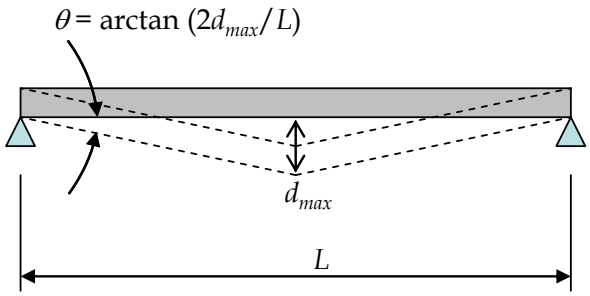

Fig. 1 Definition of Support Rotation as Function of Maximum Displacement

RESPONSE CRITERIA FOR BLAST DESIGN

The primary source of design guidance for conventionally loaded reinforced concrete wall panels is from ACI 318-11.[1] Similar design equations are provided for precast members in the PCI Design Handbook.[2] By contrast, no such universally applicable design guideline is used in the field of blast engineering. Various guidelines exist for explosive safety, anti-terrorism, and the chemical and processing industry. A component-level analysis using SDOF methods is accepted within each of these industries. However, quantitative values of support rotation

and qualitative descriptions of these response limits generally differ between the various blast guidelines. The recently published document ASCE 59-11[3] provides a summary of the different response limits used in these industries.

The response limits referenced in ASCE 59-11 are from the U.S. Army Corps of Engineers (USACE) Protective Design Center (PDC) response criteria for SDOF components.[4,5] These limits were developed for Department of Defense (DoD) facilities designed against high explosive (HE) terrorist threats. The response limits published for prestressed components in ASCE 59-11 are stated to be "*for flexural evaluation of existing components…and shall not be used for design of new elements*". Hence this study also considers non-load-bearing panel response to blast load and if existing response limits are suitable for new design.

USACE criteria define four Levels of Protection (LOP) as: High (HLOP), Medium (MLOP), Low (LLOP) and Very Low (VLLOP). These LOPs respectively correspond to expected element damage denoted as Superficial, Moderate, Heavy and Hazardous. Qualitative damage expectations for each of these four limit states per PDC TR-06-08 are provided in Table 1. Qualitative damage descriptions are nonspecific, with the same qualitative descriptions (Table 1) used for all structural components (concrete, steel, masonry, etc.).

Table 1. Qualitative Response Limits for All Structural Components (from PDC TR-06-08)

PDC TR-06-08 Damage Level	Component Consequence
B1 (HLOP)	**Superficial damage.** Component has no visible damage.
B2 (MLOP)	**Moderate damage.** Component has some permanent deflection. It is generally repairable, if necessary, although replacement may be more economical and aesthetic
B3 (LLOP)	**Heavy Damage.** Component has not failed, but it has significant permanent deflections, causing it to be irreparable.
B4 (VLLOP)	**Hazardous Failure.** Component has failed, and debris velocities range from insignificant to very significant.
> B4	**Blowout.** Component is overwhelmed by the blast load causing debris with significant velocities.

Quantitative response limits from ASCE 59-11 are provided in Table 2 for non-load-bearing prestressed concrete components. Response limits for prestressed concrete components incorporate the effect of concrete compressive strength (f'_c), the prestressing stress at ultimate moment capacity (f_{ps}), and the prestressing reinforcing ratio (A_{ps}/bd_{ps}). The displacement ductility criteria are a function of the prestressed reinforcement index, ω_p:

$$\omega_p = \frac{A_{ps}}{bd_{ps}} \frac{f_{ps}}{f'_c} \qquad \textit{Equation (1)}$$

The limits also incorporate allowance for panels with shear reinforcement. Shear reinforcing must tie two layers of flexural steel together, and meet the minimum requirements of ACI318-

11. Spacing must not be more than half the depth to the primary steel ($d/2$) along the entire member span length.

The limits in Table 2 for non-load-bearing prestressed concrete are less than published limits for reinforced concrete. Reinforced concrete components are allowed support rotations of 2°, 5°, and 10° for Moderate, Heavy and Hazardous damage levels, respectively. These limits are for single-reinforced or doubly reinforced members without shear reinforcing. If shear reinforcement is added (conforming to the requirements aforementioned) the Moderate and Heavy support rotations increase to 4° and 6°, respectively. A ductility of unity is the Superficial damage threshold for all reinforced concrete members, with no ductility limite on other damage levels.

Table 2. Non-Load-Bearing Prestressed Concrete Response Limits (from PDC TR-06-08)

Reinforcement Index	**Superficial Damage**		**Moderate Damage**		**Heavy Damage**		**Hazardous Failure**	
	μ	**θ**	**μ**	**θ**	**μ**	**θ**	**μ**	**θ**
$\omega_p > 0.30$	0.7	-	0.8	-	0.9	-	1	
$0.15 \le \omega_p \le 0.30$ or $\omega_p \le 0.15$ without shear reinforcement	0.8	-	$\frac{0.25}{\omega_p}$	1°	$\frac{0.29}{\omega_p}$	1.5°	$\frac{0.33}{\omega_p}$	2°
$\omega_p \le 0.15$ and shear reinforcement	1	-	-	1°	-	2°	-	3°

Non-load-bearing prestressed concrete limits are less than reinforced concrete members for various physical reasons. The ultimate strain of ASTM A416 prestressing strands is much less than ASTM A615 reinforcement (around 0.06 compared to 0.12[6]). The lack of strain hardening in prestressing strand also prevents the spread of plasticity once the yield displacement is reached, in contrast to ductile reinforced concrete members that exhibit widespread yielding near the location of maximum moment. Additionally, the pre-compression from prestressing reduces the available concrete strain prior to crushing.

Limits are not currently provided in blast guidelines for load-bearing prestressed concrete components, precluding their use in blast resistant design. Conversely, response limits exist for load-bearing reinforced concrete components. The response limits are limited to the Moderate damage threshold of 2° for single reinforced and doubly reinforced sections without stirrups, or 4° for doubly reinforced sections with stirrups.

Discrepancies arise in the definition of what constitutes a load-bearing element in blast design. The calculation of axial load is considered the summation of permanent static loads, and the peak dynamic reaction from any supported members (such as roof beams). Although the roof response is transient, and the peak reaction may occur over a very short time, it is conservatively treated as a permanent load. ASCE 59-11 requires axial compression forces to be considered when the axial compressive force exceeds $0.10A_g f'_c$, where A_g is the gross concrete cross-sectional area.

PDC TR-06-08 states that when axial loads exceed 20% of the dynamic axial capacity of a component, response limits are modified. For reinforced concrete members, the dynamic axial capacity is calculated as $0.20A_g f'_{dc}$, in PDC TR-06-08. This limit is supported by little research in the field of blast engineering, and is seen more as a value determined by engineering judgment. Note that the dynamic concrete compression strength, f'_{dc}, is also used in this equation, which is equal to 1.44 f'_c, accounting for dynamic and strength increase factors. Hence a member would not be considered load-bearing until the axial load exceeded 0.29 $A_g f'_c$ by PDC TR-06-08 requirements.

ANALYSIS OF PRESTRESSED CONCRETE PANELS

Blast design guidelines specify that the ultimate (plastic) capacity of prestressed concrete sections be based upon static principles, albeit using assumed dynamic increase factors for concrete and conventional steel. An elastic-plastic resistance function is commonly employed in SDOF analyses for components responding in flexure. The peak dynamic deflection is of primary interest from an SDOF analysis, and is converted to an equivalent support rotation, using the equation shown earlier in Fig. 1, and compared to quantitative criteria (such as that in Table 2). This method does not account for the actual state of stress or strain in the concrete and reinforcement when the panel reaches its maximum deflection.

SOLID PRESTRESSED CONCRETE PANELS

To determine a suitable analytical model that can be used to accurately predict prestressed member displacements (and still be used for engineering level analytical models), different resistance curves were derived for solid prestressed concrete wall panels. These methods can be used for deriving the resistance curves for both non-load-bearing and load-bearing solid panels. Three different resistance functions were considered, as follows:

1. *Elastic-Plastic with Empirical Prestress:* This resistance function uses the empirical equations from ACI 318-11 to determine the stress in the prestressing strands at ultimate capacity. This method is used by both USACE PDC and ASCE 59-11 standards, and referred to as "USACE PDC/ASCE Standards" herein. The initial stiffness is based on the average between the gross and cracked moments of inertia, following the guidelines of PDC TR-06-01.

2. *PCI Handbook Approach:* The PCI Design Handbook has guidance for calculating the cracked and ultimate static moment capacity and deflections of prestressed members. The initial stiffness up to the cracking strength is based on the gross moment of inertia. Between the cracked and ultimate moment, an empirical equation (PCI Equation 5-78) is used to determine the cracked moment of inertia. The ultimate moment is calculated using strain compatibility, where the prestressing force is based on PCI Design Aid 15.3.3, an idealized stress-strain curve for low-relaxation prestressing strand. The

resistance curve has zero stiffness once the ultimate moment is reached. This method is referred to as "PCI Design Aid: 15.3.3" in the figures that follow.

3. *Multi-Linear Approach:* Using engineering stress-strain curves for concrete, reinforcing steel and prestressing strands, a moment-curvature analysis method was developed. Non-linear material models and an analytical approach are described in detail elsewhere.[7] In this analysis method, concrete crushing and potential strand fracture are captured in the resistance curve. The strand fracture strain is taken as 0.06, an average of the range of 0.05 to 0.07 specified in the PCI Design Handbook.

Fig. 2 plots the resistance curves needed for a SDOF analysis of a solid prestressed panel using the methods described. These resistance curves are based on wall specimens used in the experimental work that follows in this paper. Walls span 16 ft between simple bearing supports. The wall specimen is 4 ft wide and 6 inches thick. Reinforcement consists of five ⅜-inch diameter Grade 270 prestressing strands placed concentrically. Welded wire reinforcement (WWR) 6 × 6-D4 × D4 is also added at mid-thickness. The cross-section described is constant along the panel height.

It is evident from the curves plotted in Fig. 2 that the moment-curvature approach predicts support rotations without failure far in excess of that allowed per Table 2 ($\omega_p \leq 0.15$ without shear reinforcement). One of the benefits with using a moment-curvature approach is that damage to WWR, prestressing strand, and concrete can be quantified with increasing support rotations. In the plot shown in Fig. 2, the WWR yields at 2°, and the peak concrete stress and maximum resistance is not reached until a support rotation of 4.8° is reached.

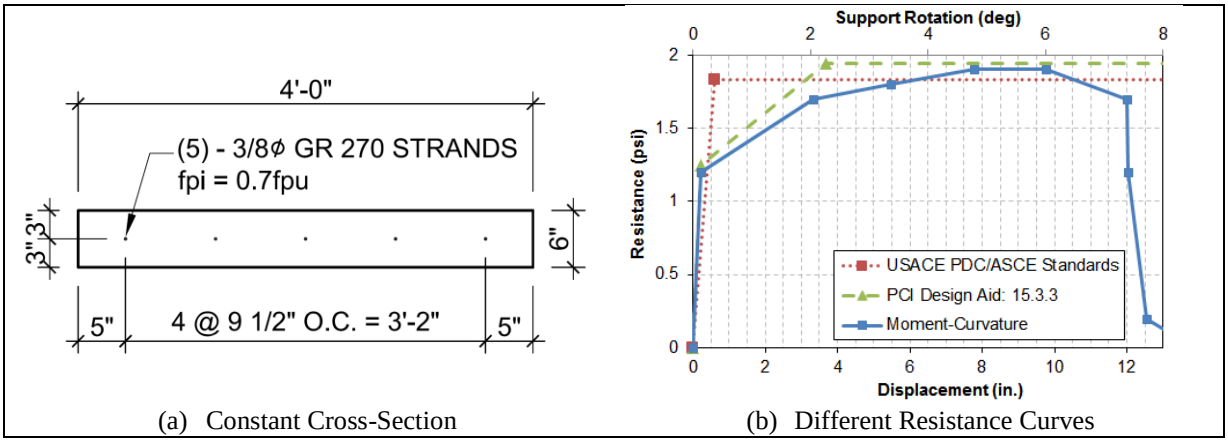

(a) Constant Cross-Section (b) Different Resistance Curves

Fig. 2 Simply-Supported 16 ft Non-Load-Bearing Solid Prestressed Concrete Panel

For the same solid prestressed panel supporting a concentric axial load of $0.1f'_cA_g$, resistance curves are plotted in Fig. 3. The resistances are calculated using the same methods, but accounting for the presence of axial load when determining internal forces and corresponding moments. A magnitude of $0.1f'_cA_g$ is used in the calculation of the resistance curve, which is the threshold used in ASCE 59-11 for reinforced concrete components. It was determined through analysis (not included in this paper) that using the PDC TR-06-08 threshold of

$0.20A_g f'_{dc}$ would be significantly un-conservative, as axial effects are detrimental at lower levels of axial load. This is a result of the initial compression from prestressing, effectively placing $0.05A_g f'_c$ axial load on the cross-section, and secondary moments.

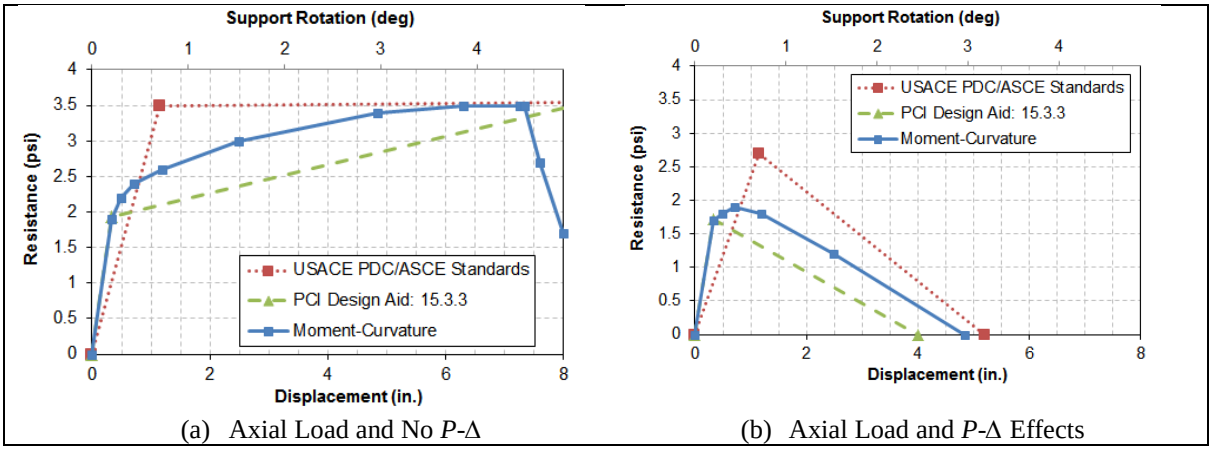

(a) Axial Load and No *P*-Δ (b) Axial Load and *P*-Δ Effects

Fig. 3. Simply-Supported 16ft Load-Bearing Solid Prestressed Concrete Panel

The secondary moments are from geometric nonlinearity, known as the P-delta (*P*-Δ) effect. As illustrated in Fig. 3, the resistance to lateral load increases with the application of axial load, but when *P*-Δ effects are included, the effective resistance is reduced as the wall deflects. More importantly, the ductility is adversely affected for these wall sections analyzed. For SDOF analyses, *P*-Δ effects are typically included as part of the forcing function (blast load) as an equivalent lateral load. Hence the curves in Fig. 3(a) would be used as the resistance function in the SDOF analysis. The same peak displacement would be calculated if the resistance function of Fig. 3(b) was used in the SDOF analysis without an additional lateral load from *P*-Δ effects.

PRESTRESSED CONCRETE SANDWICH PANELS

Many analytical and experimental studies have been completed in the last ten years through the Air Force Research Laboratory (AFRL) and PCI.[8-14] These have included static and dynamic testing of sandwich panels. One of the main difficulties with sandwich panels is determining their level of composite action. Many different proprietary shear connectors constructed from different materials (carbon fiber, glass fiber, stainless steel, galvanized steel etc.) are available, and used in the industry.

Static force-deformation experiments on various shear ties by other researchers[15] concluded that connectors have marked differences in strength, stiffness, and ductility. These parameters affect the level of composite action that can be achieved from shear transfer, and whether this force can be sustained at high support rotations. Incorporating these variables for a single set of response criteria is not viable. Hence analytical models derived assume full composite action, or a constant level of partial composite action throughout the entire resistance curve.

Composite action is determined by equating the available cumulative shear tie capacity over

half the member span to the maximum internal force developed in each wythe. An elastic shear flow (VQ/I) analysis is not appropriate in blast design, as plasticity is expected, and the moment of inertia is not constant along the member span or throughout the dynamic response. Three different resistance curve models were developed for sandwich panels, with details of the models provided below.

1. *Empirical Prestressing:* This resistance function uses the empirical equations from ACI 318-11 to determine the stress in the prestressing strands at ultimate capacity. Elastic-plastic resistance functions are determined independently for the interior and exterior wythes, from which they are combined to form a "stacked" resistance function. Similarly, an elastic-plastic resistance function is calculated for the cross-section assuming full composite action. Using a weighted resistance function, the designer can choose the degree of composite action, based on the shear tie connectors and quantity being used.

2. *PCI Handbook Approach:* Similarly to the first method described for sandwich panels, this method calculates the individual wythe resistance functions, and the full composite section to develop a weighted resistance function. The key difference between the two methods is that this method includes the cracking capacity of the section, and calculates the yield moment based on PCI Eqn 5-78. The ultimate moment is calculated using strain compatibility, where the prestressing force is based on PCI Design Aid 15.3.3, an idealized stress-strain curve for low-relaxation prestressing strand.

3. *Full Composite Multi-Linear:* In this method, full composite action is assumed between wythes throughout the entire out-of-plane response of the wall. It is recognized that this is unlikely in practice, particularly at large displacements; hence a modification factor may be required to reduce the resistance values. A moment-curvature analysis is used as the basis for developing the resistance function, including the effects of concrete crushing and strand fracture. The full composite curve is reduced by the ratio of available shear tie capacity to the required to obtain full composite action.

Fig. 4 plots the resistance curves needed for a SDOF analysis of a prestressed sandwich panel using the methods described above. These resistance curves are based on wall specimens used in the experimental work that follows in this paper. Walls span 16 ft between simple bearing supports. The wall specimen is 4 ft wide and 8 inches thick, with 3-inch concrete wythes separated by 2 inches of extruded polystyrene foam. Reinforcement consists of three ⅜-inch diameter Grade 270 prestressing strands placed concentrically in each wythe. WWR 6 × 6-D4 × D4 is also added at mid-thickness of each wythe. The wythes are connected with two welded wire girders. The specified girder depth is 5.5 inches, with continuous 0.306-inch diameter top and bottom wires. The top and bottom wires are connected with 0.243-inch diameter diagonal wires with 7.875-inch spacing between panel points. The cross-section described is constant along the panel height.

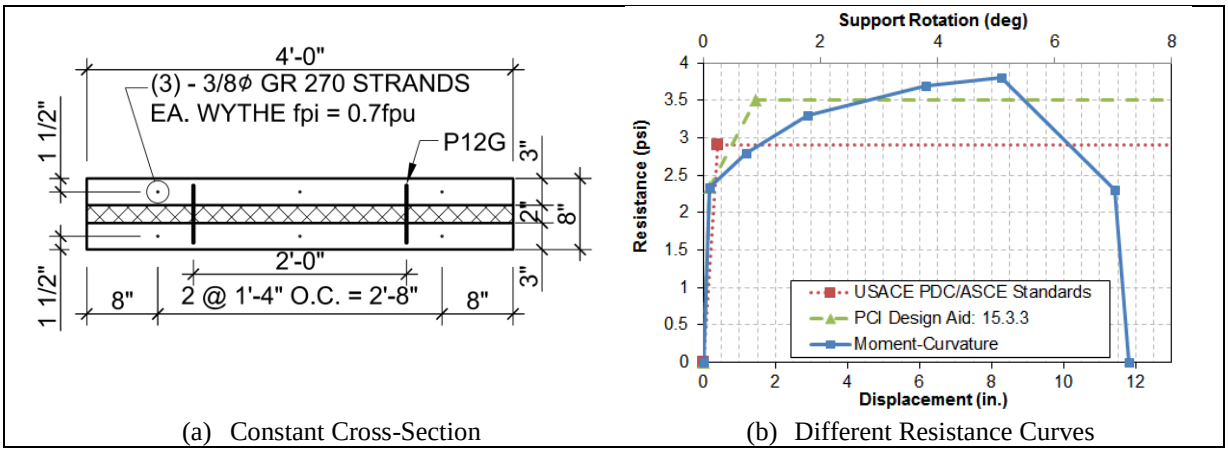

(a) Constant Cross-Section (b) Different Resistance Curves

Fig. 4. Simply-Supported 16 ft Non-Load-Bearing Prestressed Concrete Sandwich Panel

For the same prestressed sandwich panel, an applied axial load of $0.1f'_cA_g$ is used in the calculation of the resistance curve. As previously described, this axial load is treated statically as the summation of the permanent dead and live loads and peak dynamic reaction of roof components. In practice, the interior wythe would support the permanent loads, while the dynamic roof reaction would be transferred through both wythes under dynamic response. The interior eccentric load counteracts the direction of blast loading, benefiting the blast response. Therefore it is conservative to assume the combination of permanent and dynamic axial load acting through the centroid of the cross section. Resistance curves for the same prestressed sandwich panel cross-section previously described with static axial load are plotted in Fig. 5.

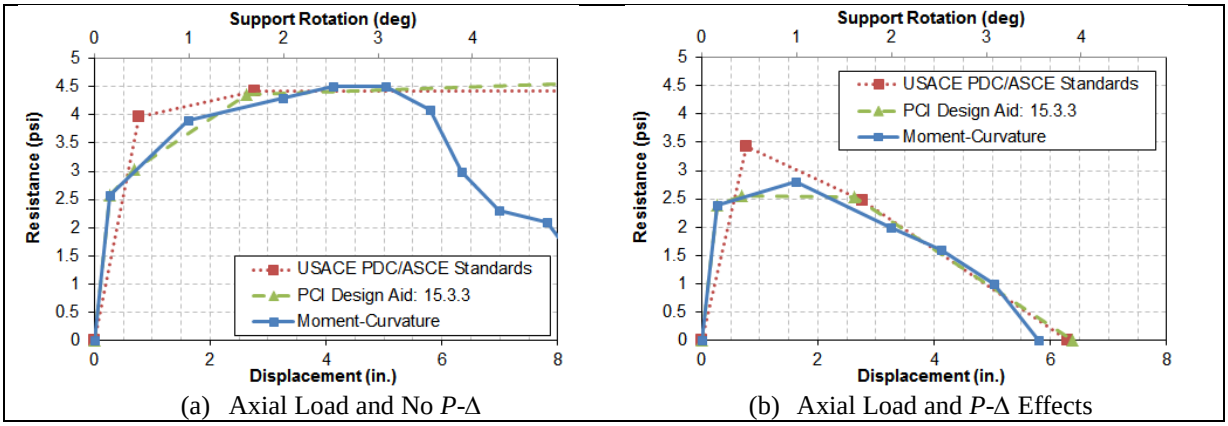

(a) Axial Load and No *P*-Δ (b) Axial Load and *P*-Δ Effects

Fig. 5. Simply-Supported 16 ft Load-Bearing Prestressed Concrete Sandwich Panel

The load-bearing solid prestressed curves of Fig. 3(a) have a larger ductility at ultimate than the load-bearing sandwich panel curves of Fig. 5(a) when *P*-Δ effects are not included in the resistance curves. However, the sandwich panel described has greater resistance than the solid prestressed panel, meaning the same *P*-Δ moment is more detrimental on the solid prestressed panel. Hence when *P*-Δ effects are included in the sandwich panel (Fig. 5b), its failure deflection is actually higher than the solid prestressed panel (Fig. 3b). This demonstrates that developing load-bearing response criteria requires consideration of the resistance-to-*P*-Δ ratio.

ANALYTICAL HYSTERESIS

Present blast modeling of conventional and prestressed concrete components uses elastic unloading in the SDOF equation of motion. This is not representative of the unloading observed in conventional concrete components, which experience stiffness degradation with increasing displacement. Prestressed components have lower residual displacements than similar reinforced concrete members due to the re-centering ability of the prestressing strands, which have a high elastic stress limit and cause concrete cracks to close. Permanent displacements become important for post-damage assessment of load-bearing components in calculating their stiffness and ability to carry static conventional loads. The disadvantage to re-centering is reduced energy dissipation, an important characteristic for seismic systems subjected to multiple reversed cyclic loading.

Characterization of the unloading stiffness and hysteretic performance of reinforced concrete beams has been studied experimentally.[16] Similar analytical models have been used on reinforced concrete wall panels loaded dynamically in shock tube tests.[7] Conversely, limited research focusing on out-of-plane hysteretic prestressed wall behavior exists, particularly for load-bearing wall systems. For this research, the moment-curvature models use a re-centering approach, assuming no residual displacement while the prestressing strand remains elastic. The exception exists when mild steel yields, to where the unloading slope is reduced by a factor of $\mu^{-0.6}$, where μ is the ductility of the conventional steel at unloading. Fig. 6 plots an elastic-plastic system using customary elastic unloading compared to a moment-curvature model with a re-centering unloading and WWR yielding. The residual displacements are significantly different, and the elastic-plastic model assumes a higher level of energy dissipation than observed in prestressed systems.

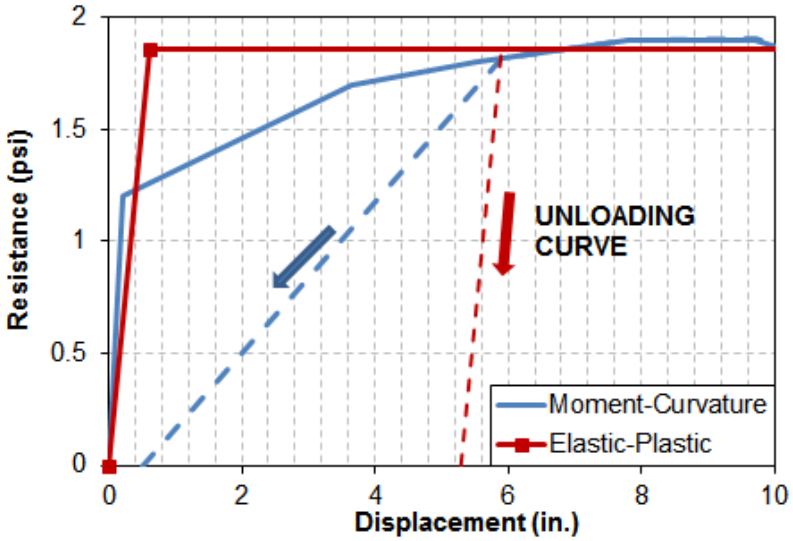

Fig. 6. Analytical Unloading Model Comparisons

EXPERIMENTAL STUDY

Nine different precast prestressed panel specimens were tested in the BakerRisk shock tube. The overall objective of the test program was to subject various precast prestressed wall panels to Moderate (M) and Heavy (H) damage levels. Table 3 describes the panel specimens used for the shock tube test matrix. Analytical models and resistance curves previously presented in this paper apply to the wall specimens in Table 3.

Table 3. Panel Specimens for Shock Tube Tests

Panel Type	Targeted Response	Axial Load	Panel Construction
Solid Prestressed	M	None	6-inch thick panel with five 3/8-inch dia. Gr 270 strands at mid-depth ($\omega_p = 0.15$) and WWR 6 × 6-D4 × D4 at mid-depth. f'_c = 7200 psi
	M	$0.10f'_cA_g$	
	H	$0.10f'_cA_g$	
Prestressed Sandwich – 100% Composite Strength	M	None	3/2/3 panel, with three 3/8-inch dia. Gr 270 strands and WWR 6 × 6-D4 × D4 mid-depth in each wythe. Two continuous P12G welded wire girders (0 gauge top and bottom wire, 3 gauge diagonal). f'_c = 7000 psi
	M	$0.10f'_cA_g$	
	H	$0.10f'_cA_g$	
Prestressed Sandwich – 60% Composite Strength	M	None	Same design as 100% composite but with 60% of shear connectors. f'_c = 6900 psi
	M	$0.10f'_cA_g$	
	H	$0.10f'_cA_g$	

All specimens were full-scale 4-ft wide panels spanning 16 ft between supports, representative of typical interstory building heights. Panels were cast by a certified PCI precaster. Sandwich panels were constructed with a bond breaker between the concrete wythes and insulation. This was purposely done to simulate potential long term bond loss or poor cohesion (oil on foam) in casting. Concrete with a compressive strength of 5000 psi was specified for all panel specimens. At the time of shock tube testing, compression strengths were measured. The average compression strength of three 6" × 12" concrete cylinders are reported in Table 3.

EXPERIMENTAL SETUP

Fig. 7 shows the BakerRisk shock tube with a single panel specimen mounted at the end of the 16 ft high × 10 ft wide expansion section. The 3-ft open width on the sides of the panel specimen were covered with steel plate bolted to the shock tube frame, and stiffened along the free edge with vertical HSS sections to reduce blast clearing. Blast clearing occurs when an incident blast wave strikes a wall of finite size in a normal orientation, and rarefaction waves are created at the edges of the wall. These rarefaction waves sweep inward from the sides, resulting in reduced overpressures and overall reduction in applied impulse.[17] A slight (¼-inch) gap was left between the vertical edges of the panels to prevent any form of contact to the test frame under dynamic response. Fig. 7(a) shows a non-load-bearing panel prior to testing, and Fig. 7(b) shows a load-bearing specimen with the axial load apparatus at the top of the wall.

The axial load applicator is the first known of its kind. Traditionally, researchers use hydraulic actuators, but these do not respond fast enough under dynamic loading to maintain a constant axial load. The apparatus shown utilizes air bladders that are contained within a fixed steel chamber, which applies force to vertical steel pistons. The pistons apply load to a spreader beam, in turn loading the top of the wall.

(a) Non-Load-Bearing Wall (b) Load-Bearing Wall

Fig. 7 Wall Specimens Mounted in Shock Tube

Connections were simple bearing connections, to eliminate connection variability from the dynamic response. As is the case with shear tie connectors, various proprietary panel-to-superstructure connections exist in the precast industry. It was not deemed practical to consider different connections in this study, or to place bias on a single type of connector. A separate shock tube test program[18] on conventionally reinforced precast with various precast connections saw panel support rotations reach 12 degrees without observing connection failure. The connections were designed using LRFD, following the equations of the PCI Design Handbook. The design load demand was set equal to the reaction associated with the ultimate dynamic resistance of the panels. Precast test panel connections designed by this method only failed in one case out of 14 tests.

Displacements were measured using an accelerometer at panel mid-height. These measurements were confirmed by overlaying a semi-transparent photo of a ½-inch grid on the side-elevation high-speed (HS) video recordings for each panel. Additional HS and high-definition (HD) videos were taken from the front elevation. Photographs were taken before and after each test, and cracks were traced with markers to increase visibility in the photographs. Whenever possible, multiple (repeat) tests were conducted on the same panels after observing panel damage to maximize the amount of data produced from this research.

EXPERIMENTAL RESULTS

Residual Support Rotations

Fig. 10 plots the experimentally measured peak and residual support rotations for both undamaged and retested panels. Linear trend lines are plotted separately for the solid prestressed (PS) and sandwich panels. Both non-load-bearing (NLB) and load-bearing (LB) results are included on the same curve. Both trend lines show an increasing difference between peak and residual support rotations with increasing maximum support rotations.

The residual support rotations for the sandwich panels are significantly higher than for the solid PS panels. Considering the analytical resistance curve of Fig. 2 for the solid PS panel, the WWR yields at a support rotation of approximately 2° and prestressing begins to yield at 3.4° support rotation. For the sandwich panel case with analytical resistance curves of Fig. 4, the WWR yields much earlier at a support rotation of 0.7° and the strand yields at 1.8° support rotation. More importantly, both curves illustrate that low levels of residual deflection occur in both specimens. This supports a re-centering hysteresis model previously described, rather than an elastic-plastic model which would predict high residual displacements, only slightly less than the peak displacement.

Table 4 provides a summary of the experimental data for all tests. The results are divided into panel type, rather than in test number order. Although only nine panel specimens were available, twenty shock tube tests were completed. Panels that were tested multiple times are indicated in Table 4 with an asterisk. The table includes peak pressure, applied impulse, peak mid-height displacement Δ_{max}, peak support rotation θ_{max}, residual mid-height displacement $\Delta_{res,}$ residual support rotation θ_{res}, and a qualitative description of damage. For brevity, full test descriptions and observations were not included in this paper. Undamaged panels are classified as those with no prior testing; namely Tests 1, 10 and 15 for solid prestressed panels, Tests 5, 12 and 17 for 100% composite sandwich panels, and Tests 7, 13 and 20 for 60% composite sandwich panels. The next subsections focus on key insights gained from the experimental program.

Peak Support Rotations

Peak displacements were measured and converted to idealized support rotations using the approximation shown in Fig. 1. The peak support rotations are plotted separately for the non-load-bearing solid prestressed and sandwich panels in Fig. 8 against the quantitative damage thresholds of Table 2 ($\omega_p \leq 0.15$ without shear reinforcement). Fig. 8 shows support rotations achieved, and the qualitative damage observed (Table 4) in the tests. Both plots show the prestressed panels are capable of deforming significantly above published response limits. Note that blowout did not occur for the solid prestressed non-load-bearing panel (Fig. 8a) until a support rotation of 7.4°.

Similar curves are plotted for the load-bearing solid prestressed and sandwich panels in

Fig. 9. Although published limits do not currently exist for load-bearing panels, the measured response is plotted against the non-load-bearing limits for discussion purposes. Even under a static axial load magnitude of $0.1f'_cA_g$, the walls tested are capable of displacing to the published response limits for non-load-bearing prestressed wall panels.

Residual Support Rotations

Fig. 10 plots the experimentally measured peak and residual support rotations for both undamaged and retested panels. Linear trend lines are plotted separately for the solid prestressed (PS) and sandwich panels. Both non-load-bearing (NLB) and load-bearing (LB) results are included on the same curve. Both trend lines show an increasing difference between peak and residual support rotations with increasing maximum support rotations.

The residual support rotations for the sandwich panels are significantly higher than for the solid PS panels. Considering the analytical resistance curve of Fig. 2 for the solid PS panel, the WWR yields at a support rotation of approximately 2° and prestressing begins to yield at 3.4° support rotation. For the sandwich panel case with analytical resistance curves of Fig. 4, the WWR yields much earlier at a support rotation of 0.7° and the strand yields at 1.8° support rotation. More importantly, both curves illustrate that low levels of residual deflection occur in both specimens. This supports a re-centering hysteresis model previously described, rather than an elastic-plastic model which would predict high residual displacements, only slightly less than the peak displacement.

Table 4. Experimental Results

Test	**Axial (kips)**	**P (psig)**	**i (psi-ms)**	**Δ_{max} (inch)**	**θ_{max}**	**Δ_{res} (inch)**	**θ_{res}**	**Observed Damage**
6-inch Solid Prestressed Panel: (5)-⅜″ GR 270 Strands Concentric								
1	0	4.2	78	1.8	1.1°	0.2	0.1°	Hairline Cracking (Superficial)
2*	0	5.6	103	4.2	2.6°	0.4	0.25°	Widespread Cracking (Moderate)
3*	0	5.8	112	5.9	3.6°	0.5	0.3°	Widespread Cracking (Heavy)
4*	0	6.9	146	Fails ~ 12	7.4°	-	-	Strand Fracture (Blowout)
10	144	5.8	114	2.3	1.4°	0.1	0.1°	Cracking & perm. def. (Moderate)
11*	144	6.4	127	3.1	1.9°	0.3	0.1°	Cracking & perm. def. (Moderate)
15	144	7.0	128	3.4	2.1°	0.44	0.2°	Cracking & perm. def. (Moderate)
16*	144	7.3	135	Fails ~ 5.5	3.4°	-	-	Blowout
100% Ultimate Strength 3/2/3 Sandwich Panel: (3)-⅜″ GR 270 Strands Concentric each wythe								
5	0	6.4	122	2.3	1.4°	0.8	0.5°	Cracking & perm. def. (Moderate)
6*	0	6.9	138	4.8	3.0°	1.6	1°	Cracking & prestress bond failure cracks (Heavy)
12	144	7.1	148	Fails ~ 7	4.3°	-	-	Blowout

17	144	4.5	75	1.3	0.8°	0	0°	No visible cracks (Superficial)
18*	144	5.6	93	1.9	1.2°	0.44	0.3°	Cracking & perm. def. (Moderate)
19*	144	6.4	115	3.3	2.0°	1.1	0.65°	Cracking & significant permanent deflection (Heavy)
60% Ultimate Strength 3/2/3 Sandwich Panel: (3)-⅜″ GR 270 Strands Concentric each wythe								
7	0	4.2	79	1.5	0.9°	0.3	0.2°	Cracking & perm. def. (Moderate)
8*	0	6.4	125	4.3	2.6°	0.9	0.6°	Large perm. def. (Moderate/Heavy)
9*	0	7.1	150	7.0	4.3°	1.3	0.8°	Large perm. def. (Moderate/Heavy)
13	144	4.4	77	1.5	0.9°	0	0°	Hairline Cracking (Superficial)
14*	144	5.3	97	2.5	1.5°	0.5	0.3°	Cracking & perm. def. (Moderate)
20	144	6.8	123	3.3	2.0°	1.1	0.7°	Cracking & significant perm. def. (Heavy)

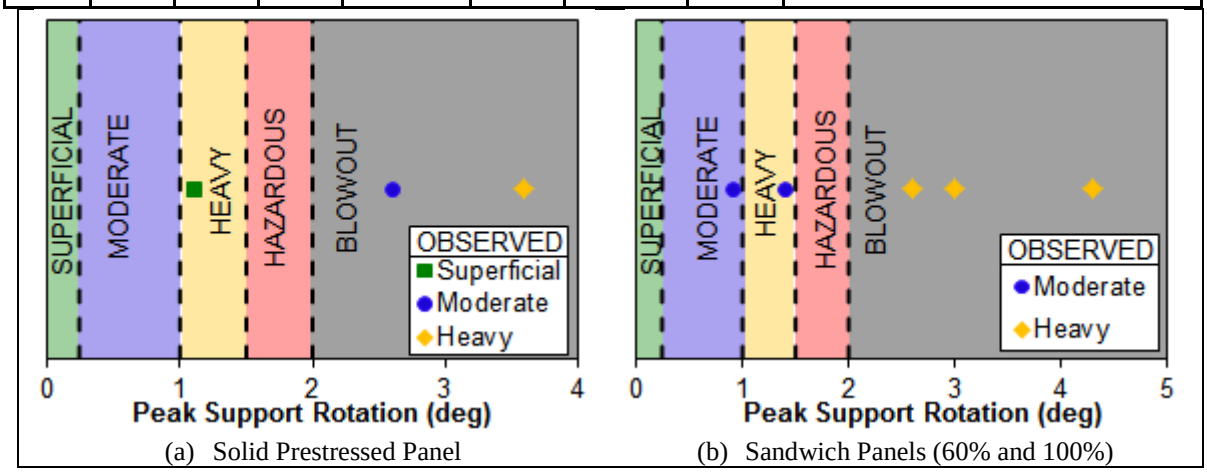

(a) Solid Prestressed Panel (b) Sandwich Panels (60% and 100%)

Fig. 8 Peak Support Rotations Achieved vs. Published Limits for Non-Load-Bearing Panels

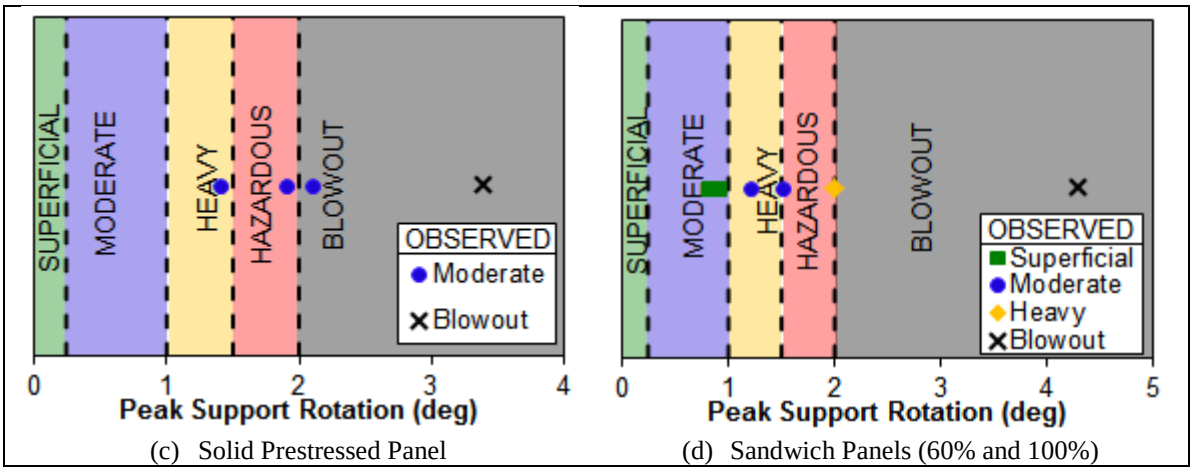

(c) Solid Prestressed Panel (d) Sandwich Panels (60% and 100%)

Fig. 9 Peak Support Rotations Achieved vs. Published Limits for Load-Bearing Panels

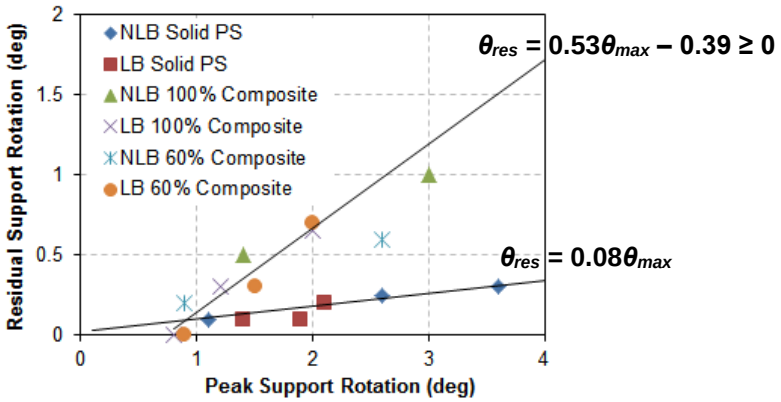

Fig. 10 Experimental Peak vs. Residual Support Rotations

Axial Load Apparatus

It is important to demonstrate that the applied axial load remained near constant throughout the dynamic tests. In contrast to hydraulic actuators that are incapable of maintaining a constant load under rapid vertical panel shortening and elongation, the air bladders are capable of expanding and contracting rapidly. Fig. 11 plots two different axial load measurements from the shock tube test program. In Test 13, the panel displaced 1.5 inches laterally, and the axial load variation was less than 4% throughout the wall dynamic response (Fig. 11a). At the other extreme, the panel in Test 12 failed catastrophically, and the panel dislodged from the shock tube. Referring to Fig. 11(b), the panel failure displacement was around 7 inches, at which time the axial load was still within 6% of the target axial load. Once the panel fails, the axial load drops off rapidly.

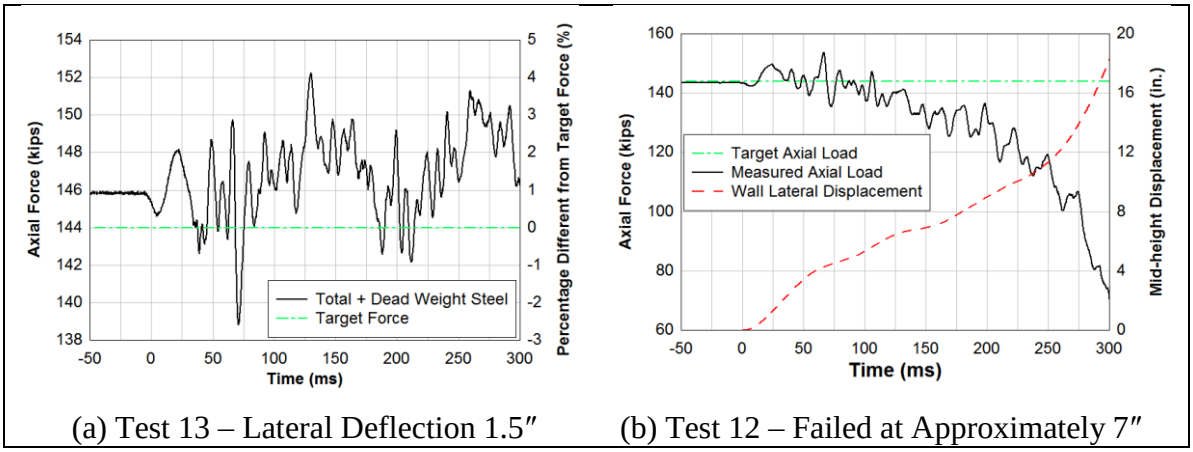

(a) Test 13 – Lateral Deflection 1.5″ (b) Test 12 – Failed at Approximately 7″

Fig. 11 Example Axial Load Measurements

ANALYSIS OF TEST RESULTS

The analytical methods presented earlier in this paper were used to model the experimental tests performed. As SDOF models are only intended for undamaged panels, panels that were retested are not modeled in this paper. Results comparing peak and residual lateral displacements are reported in Table 5. It should be noted that the moment-curvature model using the modified hysteresis rules did provide good agreement with re-tested panels.

Dynamic increase factors (DIFs) for concrete were taken as the default recommended values from blast guidelines for the empirical prestress (PDC/ASCE method) and PCI Handbook approach. For the moment curvature model, calculations were iterated to find the actual strain rates in concrete, and the corresponding value of DIF obtained from published curves.[4] This is possible with such a model, as the strains are known within a cross section at any level of displacement. For all models, the DIF for prestressing strand was taken as unity and 1.1 for WWR.

In general, the peak displacements predicted using resistance functions from the PDC/ASCE

and PCI Handbook under-predict the peak displacement. The residual displacements are over-predicted, as the elastic stiffness is used for unloading. The moment-curvature provides better agreement with peak and residual displacements. One important modification made to the moment-curvature model was assuming a non-composite section at first cracking due to the presence of bond-breaker at the wythe-to-foam interface. Shear slip is required to engage the wire truss ties before they can carry force between the wythe interface.

Table 5. SDOF Predictions for Undamaged Panels Tested

Test	Axial (kips)	Experimental Displacements (inches)		Analytical Displacements (inches)					
				PDC/ASCE		PCI Handbook		Moment-Curvature	
		Δ_{max}	Δ_{res}	Δ_{max}	Δ_{res}	Δ_{max}	Δ_{res}	Δ_{max}	Δ_{res}
6-inch Solid Prestressed Panel: (5)-⅜″ GR 270 Strands Concentric									
1	0	1.8	0.2	1.5	0.6	1.6	1.1	1.7	0.2
10	144	2.3	0.1	2.0	1.1	Fails ~ 4	-	2.3	0
15	144	3.4	0.44	2.8	1.3	Fails ~ 4	-	Fails ~ 5	-
100% Ultimate Strength 3/2/3 Sandwich Panel: (3)-⅜″ GR 270 Strands Concentric each wythe									
5	0	2.3	0.8	1.8	1.2	1.3	0.5	2.4	0.4
12	144	Fails ~ 7	-	2.5	2	3	2.8	Fails ~ 6	-
17	144	1.3	0	0.7	0.1	0.5	0.1	1.5	0
60% Ultimate Strength 3/2/3 Sandwich Panel: (3)-⅜″ GR 270 Strands Concentric each wythe									
7	0	1.5	0.3	0.9	0.5	1.0	0.7	1.7	0.2
13	144	1.5	0	0.8	0.1	0.6	0.2	1.7	0
20	144	3.3	1.1	1.8	1.2	1.7	1.3	3.5	1.4

NON-LOAD-BEARING RESISTANCE CURVE EVALUATIONS

The moment-curvature resistance curves provided good agreement with the measured shock tube test displacements. Nonetheless, the most accurate way to validate resistance functions is to statically test the same panels. As this data is not available, the peak support rotations and corresponding qualitative damage observations (Table 4) are plotted on the derived resistance curves in Fig. 12. Included in this figure are vertical lines that represent damage calculated with the moment-curvature model. Since the 60% composite curve is taken as a scalar of the 100% composite resistance curve, data points are included on the same plot in Fig. 12(b).

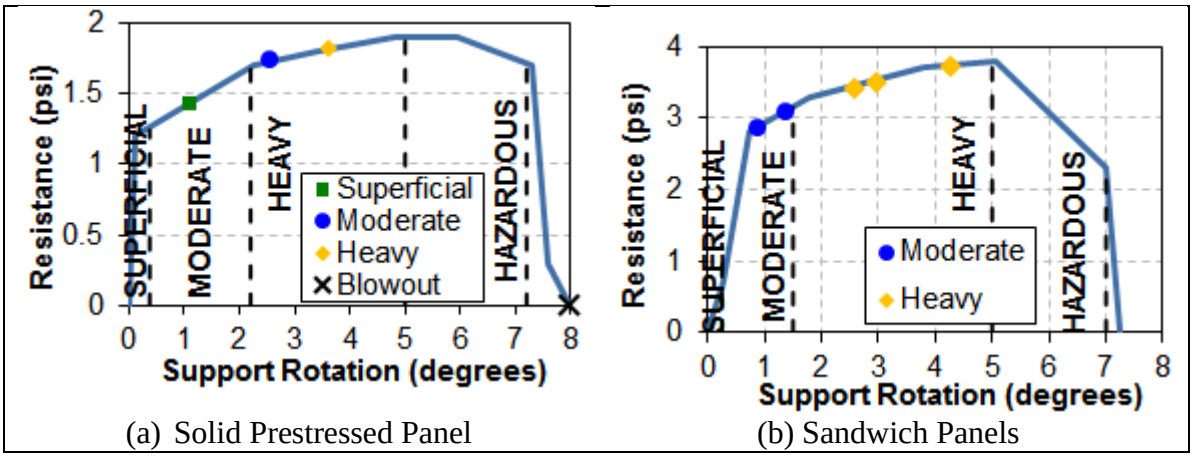

(a) Solid Prestressed Panel (b) Sandwich Panels

Fig. 12 Comparison of Non-Load-Bearing Resistance Curves and Observed Damage

The Moderate damage threshold is conservatively taken as the first yield of WWR, which will produce some residual displacement. As this displacement is typically small, the Moderate threshold could be increased to first yield of prestressing strand. The Heavy threshold corresponds to the ultimate resistance, usually associated with concrete reaching its peak stress. Finally, the Hazardous limit is defined as the resistance dropping to 80% of the ultimate resistance capacity.

Resistance curves show good agreement with observed damage states. The only outlier is Moderate damage observed in the solid prestressed panel (Fig. 12a), in the Heavy damage threshold. As previously mentioned, the Moderate threshold was conservatively set at first yield of WWR, rather than yield of prestressing strand. For this particular panel, the strand does not yield until 3.4°. If this limit had been used, the observed damage and analytical threshold would agree. Nevertheless, a conservative threshold of Moderate is set at the first yield of WWR.

Similar evaluations can be made for load-bearing resistance curves. However, these are less meaningful, as the damage levels are governed by PΔ failure modes, rather than large strains within the cross-section from pure flexure.

CONCLUSIONS AND FUTURE RECOMMENDATIONS

Based on the experimental study, and analytical findings presented in this report, the following conclusions can be made:

1. A full-scale shock tube test program demonstrated that non-load-bearing solid prestressed and prestressed concrete sandwich panels can deflect significantly higher than prescribed blast design limits. For the panels tested, Moderate and Heavy damage was observed at limits in excess of the current published Hazardous thresholds.
2. For load-bearing solid prestressed and prestressed concrete sandwich panels, panels reached support rotations in agreement of current response limits. Supporting a static

axial load of $0.1f'_cA_g$, all panel specimens were able to achieve 2° of support rotation without failure.

3. Load-bearing failure modes were governed by geometric *P*-Δ effects, rather than concrete crushing or strand fracture. This stressed the importance for *P*-Δ effects to be considered in the dynamic response of thin load-bearing elements with low resistances.
4. A multi-linear resistance function derived through a moment-curvature analysis allows for more accurate predictions of panel displacement and rotation than currently used typical elastic-plastic idealization. The moment-curvature model is significantly more reliable at predicting residual displacements than the elastic-plastic model. This is of less concern for design, but can be important in load-bearing walls, blast loads with a significant negative phase, and in post-damage assessments, such as for accident reconstructions, when only residual displacements are available.

The above conclusions are applicable to panels within the parameter limits imposed on the current study. Hence recommendations for future work include further testing with varying span length, prestressing ratios and level of axial load. Specifically, it would be beneficial for response criteria to have panels with axial loads of $0.05f'_cA_g$. Additional testing on sandwich panels with proprietary shear connectors is also of interest.

ACKNOWLEDGMENTS

This work was funded by the Precast/Prestressed Concrete Institute. A select advisory committee provided valuable guidance throughout the course of this work. Specifically, Roger Becker, Greg Force, Suzanne Aultman, Phil Benshoof, Steven Brock, James Davidson, John Geringer, John Hoemann, Clay Naito and Pat O'Brien. Recognition is also given to Coreslab Structures (Texas) Inc. for fabricating and supplying the prestressed wall specimens.

REFERENCES

1. ACI Committee 318, *Building Code Requirements for Structural Concrete (ACI 318-11) and Commentary (ACI 318-11R),* Farmington Hills, Michigan, 2011.
2. PCI Industry Handbook Committee, *PCI Design Handbook – Precast and Prestressed Concrete*, Seventh Edition, Chicago, Illinois, 2010.
3. ASCE 59-11, *Blast Protection of Buildings,* Published by the American Society of Engineers (ASCE), Reston, VA, 2011.
4. PDC TR-06-01, "Methodology Manual for the Single-Degree-of-Freedom Blast Effects Design Spreadsheets (SBEDS)," U.S. Army Corps of Engineers (USACE), Protective Design Center (PDC) *Technical Report 06-01*, Sep. 2006.
5. PDC TR-06-08, "Single Degree of Freedom Response Limits for Antiterrorism Design," USACE PDC *Technical Report 06-08*, Jan. 2008.
6. Malvar, L.J. (1998). "Review of Static and Dynamic Properties of Steel Reinforcing Bars," *ACI Materials Journal*, Vol. 95, No. 5, Sep.-Oct. 1998, pp. 609-614

7. Mander, T.J., and Polcyn, M.A. (2014). "Blast Performance and Response Limits of Non-Load-Bearing Concrete Panels," *2014 PCI Convention and National Bridge Conference*, Washington D.C.
8. Cramsey, N., and Naito, C., "Analytical Assessment of the Blast Resistance of Precast, Prestressed Concrete Components," Air Force Research Laboratory (AFRL), *Technical Report AFRL-ML-TY-TP-2007-4529*, Apr. 2007.
9. Newberry, C.M., Davidson, J., Hoemann, J., and Bewick, B.T., "Simulation of Prestressed Concrete Sandwich Panels Subjected to Blast Loads," AFRL, *Technical Report AFRL-RX-TY-TP-2010-0014*, Feb. 2010.
10. Davidson, J.S., Newberry, C.M., Hammons, M.I., and Bewick, B.T., "Finite Element Simulation and Assessment of Single-Degree-of-Freedom Prediction Methodology for Insulated Concrete Sandwich Panels Subjected to Blast Loads," AFRL, *Technical Report AFRL-RX-TY-TR-2011-0031*, Feb. 2011.
11. Cramsey, N., and Naito, C., "Analytical Assessment of Blast Resistance of Precast, Prestressed Concrete Components," *PCI Journal*, pp. 67-80, Nov-Dec 2007.
12. Naito, C.J., Dinan, R.J., Fisher, J.W., and Hoemann, J.M., "Precast/Prestressed Concrete Experiments – Series 1 (Volume 1)," AFRL, *Technical Report AFRL-RX-TY-TR-2008-4616*, Nov. 2008.
13. Naito, C.J., Hoemann, J.M., Shull, J.S., Saucier, A., Salim, H.A., Bewick, B.T., and Hammons, M.I., "Precast/Prestressed Concrete Experiments Performance on Non-Load Bearing Sandwich Wall Panels," AFRL, *Technical Report AFRL-RX-TY-TR-2011-0021*, Jan. 2011.
14. Naito, C., Beacraft, M., and Hoemann, J., "Design Limits for Precast Concrete Sandwich Walls Subjected to External Explosions," AFRL, *Technical Report AFRL-RX-TY-TP-2010-0013*, Feb. 2010.
15. Naito, C., Hoemann, J., Bewick, B.T., and Hammons, M.I. (2009). "Evaluation of Shear Tie Connectors for Use in Insulated Concrete Sandwich Panels," AFRL, *Technical Report AFRL-RX-TY-TR-2009-4600*, Dec. 2009.
16. Takeda, T., Sozen, M., A., and Nielsen, N.N. (1970). "Reinforced Concrete Response to Simulated Earthquakes," *Journal of the Structural Division*, Proceedings of the ASCE, Vol. 96, No. ST 12, Dec. 1970, pp. 2557-2573.
17. Geng, J., Mander, T.J., and Baker, Q.A., "Blast Wave Clearing Behavior for Positive and Negative Phases," *Journal of Loss Prevention in the Process Industries*, available online 24 October 2014.
18. Lowak, M.J., and Montoya, J.R., "Shock Tube Testing of Precast Concrete Panels," Prepared for Protection Engineering Consultants, Inc., *BakerRisk Project No. 01-03471-001-11*, March, 2012.